Physica E 59 (2014) 110–116

Contents lists available at ScienceDirect

Physica E

journal homepage: www.elsevier.com/locate/physe

Synthesis of ZnO nanoplates decorated rhombus-shaped ZnO nanorods and their application in solar cells

Yufu Zhu [a,*], Wenzhong Shen [b]

[a] Jiangsu Provincial Key Lab for Interventional Medical Devices, Huaiyin Institute of Technology, Huaian 223003, China
[b] Institute of Solar Energy and Key Laboratory of Artificial Structures and Quantum Control (Ministry of Education), Department of Physics and Astronomy, Shanghai Jiao Tong University, Shanghai 200240, China

HIGHLIGHTS

- Novel nanostructures of ZnF(OH) nanoplates decorated ZnF(OH) nanorods were fabricated.
- The above mentioned novel architectures have never been reported.
- Porous ZnO nanostructures were obtained by calcining the obtained ZnF(OH) ones.
- Rhombus-shaped ZnO nanorods and complex ZnO nanostructures were used in solar cells.
- The complex ZnO nanostructures show superior photoelectric conversion performance.

GRAPHICAL ABSTRACT

ZnF(OH) nanoplates decorated ZnF(OH) nanorods were fabricated. Hierarchical porous ZnO were obtained by calcining the obtained nanostructures. The yielded ZnO shows superior photoelectric conversion performance.

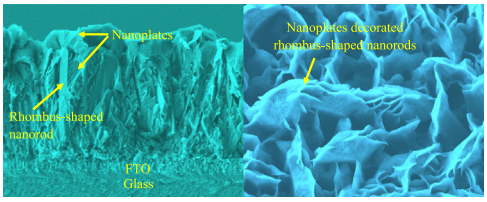

ARTICLE INFO

Article history:
Received 22 November 2013
Received in revised form
24 December 2013
Accepted 7 January 2014
Available online 15 January 2014

Keywords:
Semiconductor nanostructure
Chemical synthesis
Photovoltaic application

ABSTRACT

Novel nanostructures of ZnF(OH) nanoplates decorated rhombus-shaped ZnF(OH) nanorods were fabricated. The obtained precursors were transformed by calcination to porous hierarchical ZnO nanostructures with the original morphologies retained. Field emission scanning electron microscope images exhibit that the nanoplates are grown in the interstices between the nanorods and on the top of the nanorods. The structure and composition of the obtained products have been confirmed by transmission electron microscope and X-ray diffraction measurements. The obtained ZnO nanostructures have been successfully used in solar cells. The light-to-electricity conversion results show that the complex nanostructures exhibit a power conversion efficiency of 1.36% with a photoelectrode thickness of 4.2 μm, which is comparable to those based on 40 μm vertically aligned hexagonal-shaped ZnO nanowire array photoelectrodes. These results indicate that the synthesized ZnO nanoplate decorated rhombus-shaped ZnO nanorod nanostructures are more suitable for application as a photoelectrode in solar cells.

1. Introduction

Development and utilization of new energy is an important approach to cope with energy shortage. As a new generation solar cell, dye-sensitized solar cells (DSCs) have aroused more and more interest for its advantages of non-toxicity, ease of fabrication and cost-effectiveness. However, the overall efficiency of DSCs has been lower than silicon-based solar cells. More research is being done to improve the efficiency of DSCs [1–18]. Among the variety of photoelectrode materials used in DSCs, the synthesis and application of ZnO nanostructures in solar cells have attracted much attention due to their abundance on earth, eco-friendliness

* Corresponding author. Fax: +86 517 83559130.
E-mail address: yufu_zhu@163.com (Y. Zhu).

1386-9477/$ - see front matter © 2014 Elsevier B.V. All rights reserved.
http://dx.doi.org/10.1016/j.physe.2014.01.010

and feasibility for fabrication [1–8]. As we all know, the morphology and surface area of nanostructure play an important role in determining the efficiency of the solar cells. Therefore, much effort has been directed toward the design and synthesis of novel ZnO nanostructures with high surface area for improving the performance of solar cells.

Upto now, ZnO nanostructures with various morphologies including nanowires [9–13], nanorods [14], nanotubes [15], nanosheets [16], nanoflowers [17] and nanotetrapods [18] have been synthesized and applied in DSCs. Among the above mentioned various nanostructures, the synthesis and application of ZnO nanowires in solar cells are of great interest due to the fact that the nanowire has been shown to provide a direct conduction pathway for the photogenerated electrons [9–13]. Recently, the synthesis of rhombus-shaped porous ZnO nanorods has been realized [19–22]. The rhombus-shaped nanorod based DSCs have demonstrated improved photoelectric conversion performance compared with the conventional hexagonal-shaped ZnO nanowire counterpart [21,22]. Actually, the efficiency of the solar cells based on rhombus-shaped nanorods can be further improved if the synthesis of more complex nanostructures can be realized. Thus, it still remains a significant challenge to optimize the structural design that may greatly improve the overall efficiency of the solar cells.

In this paper, a novel porous structure of ZnO nanoplates decorated rhombus-shaped ZnO nanorods has been synthesized by a facile hydrothermal method combined with subsequent calcinations. The unique morphology of the novel nanostructures has the advantage of possessing large surface area. For potential applications, such hierarchical nanostructures should exhibit excellent performance in solar cells, photocatalysis, and gas sensors. To the best of our knowledge, such a novel ZnO architecture obtained via a simple and low-cost chemical method used in developing solar cells has never been reported. During the synthesis process, hierarchical nanostructures consisting of rhombus-shaped ZnF(OH) nanorods and ZnF(OH) nanoplates were firstly synthesized. After calcination, the synthesis of hierarchical porous ZnO nanostructures consisting of rhombus-shaped ZnO nanorods and ZnO nanoplates can be realized. Interestingly, the novel architecture consists of mesoporous ZnO nanoplates which are interconnected with each other to form a macro-porous network. Benefiting from the porous structures as well as enhanced dye loading of the photoelectrodes, DSC based on such photoelectrode exhibits a power conversion efficiency (PCE) of 1.36% with a photoelectrode thickness of 4.2 μm, which is comparable to those based on 40 μm vertically aligned hexagonal-shaped ZnO nanowire array photoelectrode, as previously reported in Ref. [11].

2. Experimental details

2.1. Synthesis of ZnO nanostructures with various morphologies

FTO glass substrates were alternately cleaned ultrasonically in deionized water and absolute ethanol for 10 min each. The total cleaning process was repeated two times. A layer of ZnO seed was formed on the substrate using a sol–gel dip coating method, followed by thermal decomposition at 500 °C for 60 min. The ZnO sol used here was $Zn(CH_3COO)_2$ (0.3 M) in a mixed solvent of ethanol and ethanolamine. The seeded substrate was placed in an aqueous solution containing 0.03 M $Zn(NO_3)_2 \cdot 6H_2O$ and 0.3 M NH_4F, which was sealed in a Teflon-lined stainless steel autoclave and maintained at 120 °C. The detailed synthesis conditions for nanostructures of various morphologies (film nos. 1–4) were described in Table 1.

In order to clearly demonstrate the growth process of the nanostructures, similar growth conditions were adopted except for that the growth time was set as 2, 5 and 8 h (film nos. 1–3 in Table 1).

Table 1
Preparation conditions for various nanostructure films 1–4.

Films	Substrates used for nanostructure growth	Zn $(NO_3)_2 \cdot 6H_2O$ (M)	NH_4F (M)	Temperature (°C)	Time (hr)
No. 1	ZnO seeded FTO	0.03	0.3	120	2
No. 2	ZnO seeded FTO	0.03	0.3	120	5
No. 3	ZnO seeded FTO	0.03	0.3	120	8
No. 4	Film no. 1	0.03	0.3	120	14

In order to increase the thickness of the nanostructures grown on FTO substrate, a two-step growth process was also used. Step one, ZnF(OH) nanorod arrays on FTO substrate was synthesized by immersing the seeded FTO substrate in the above mentioned solution for 2 h (film no. 1). Step two, the step-one prepared sample was immersed in a fresh growth solution for another 14 h (film no. 4). After the reaction, the FTO substrates with nanostructures grown on them were taken out and rinsed with deionized water for several times to remove any residual chemicals absorbed on the surfaces of the nanostructures. Finally, all the obtained products were calcinated at 500 °C for 2 h in a furnace to transform the obtained products to ZnO. During the calcination process, the furnace should be put in a high efficient fume hood because poisonous HF will be produced during this process.

2.2. Structural characterization

During the morphology characterization, a focused ion beam (FIB; Auriga 60) was used for cross-sectional sample preparation. The morphology and structure of the obtained nanostructures were characterized using a Field emission scanning electron microscope (FESEM; JEOL JSM-7400F OR Auriga 60) and a transmission electron microscope (TEM; JEOL JEM-2010F). X-ray diffraction (XRD) was carried out on a Rigaku D-Max B diffractometer equipped with a Cu K_α source ($\lambda = 1.5406$ Å).

2.3. Fabrication and photovoltaic measurement of DSCs

Before being assembled into DSCs, the FTO substrates with ZnO nanostructures grown on them were transferred into a 0.5 mM N719 dye solution in anhydrous ethanol for 2.5 h for dye loading. FTO with a layer of sputtered Pt was used as the counter-electrodes. The dye-sensitized photoelectrodes and counter-electrodes were then separated by a spacer (25 μm in thickness) and pressed with clamps. The electrolyte of 0.6 M tetra-butylammonium iodide, 0.1 M lithium iodide, 0.1 M iodine, and 0.5 M 4-tert-butylpyridine in acetonitrile was introduced into the two electrodes by a plastic dropper and capillary action. An oriel solar simulator was used as a white light source. The intensity of the incident light was calibrated to be 100 mW cm^{-2} by a S1787 Hamamatsu silicon cell. The photocurrent–photovoltage curves were measured using a computer-controlled Keithley 2400 source meter by varying the external load voltage. A mask with an aperture area of 0.125 cm^2 was employed during the measurements for the calibration of the cell area.

3. Results and discussion

3.1. Morphology and structure of the as-grown Zn(OH)F nanorod arrays

Fig. 1(a) shows the XRD patterns of the 2 h grown nanostructures on the FTO substrate (the detailed growth conditions were described in the film no. 1 in Table 1). The peaks marked with solid

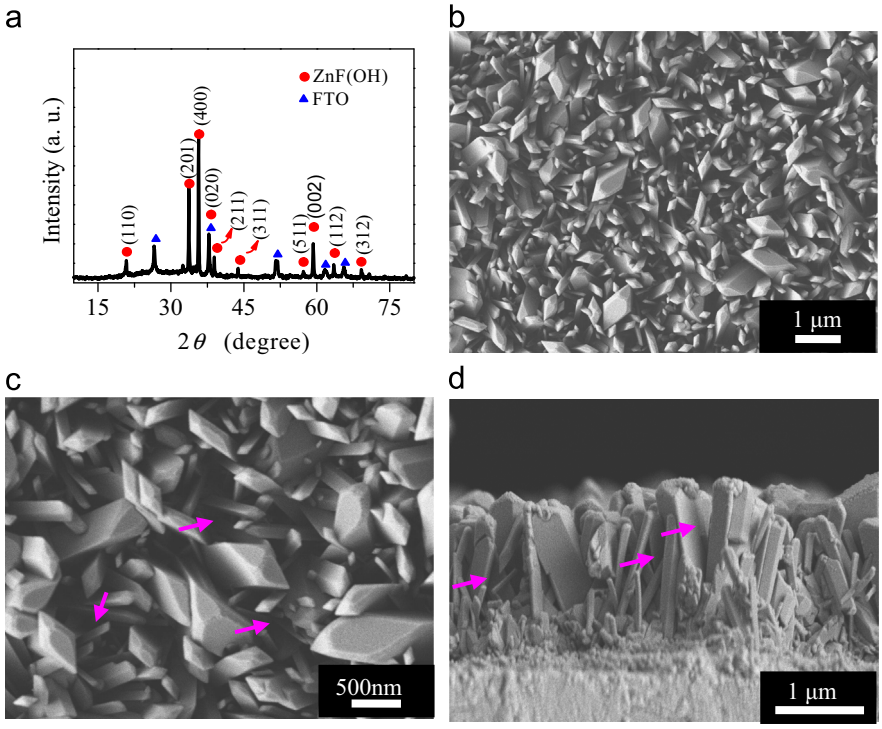

Fig. 1. (a) XRD pattern, (b) low- (c) high-magnification top-view SEM image and (d) cross-section SEM image of the Zn(OH)F nanorod arrays. This sample is corresponding to the film no. 1 described in Table 1.

circles are consistent with those of orthorhombic Zn(OH)F [Joint Committee for Powder Diffraction Standards (JCPDS) no. 32-1469]. The other peaks marked with solid triangle are arising from the FTO substrate. No other peaks were detected, implying the absence of any impurities in the ZnF(OH) nanorod array film.

Fig. 1(b)–(d) shows the typical morphology of the as-synthesized ZnF(OH) nanorod arrays on FTO substrate. As can be seen in Fig. 1(b), a high density of ZnF(OH) nanorods were grown on the FTO substrate. A high-magnification SEM image of the nanorod array demonstrated in Fig. 1(c) clearly shows that the obtained nanorods have a clear-cut rhombic contour with edge lengths ranging from tens of nanometers to hundreds of nanometers. The cross-sectional SEM image of the Zn(OH)F nanorods array grown on FTO in Fig. 1(d) reveals good alignment of the nanorod array with a thickness of about 2 μm. The following reactions are involved during the formation of the preferentially oriented Zn(OH)F nanorod array:

$$Zn^{2+} + F^{-} \leftrightarrow ZnF^{+} \quad (1)$$

$$ZnF^{+} + OH^{-} \leftrightarrow Zn(OH)F \quad (2)$$

As described in Table 1, ZnO seeded FTO was used for Zn(OH)F nanorod array growth. The ZnO seed layer used here will facilitate the growth of Zn(OH)F nanorod on FTO substrate. During the experimental process, we found that there was no Zn(OH)F nanorod array growth on FTO if bare FTO substrates were used for nanostructure deposition.

Although the density of the nanorods is very high, there are large interstices between the nanorods, as demonstrated by the arrows shown in Fig. 1(c) and (d). If the interstices between the ZnF(OH) nanorods can be filled by the other nanostructures, the surface area of this kind of nanostructure would be increased. As we all know, large surface area of a photoelectrode is one of the critical factors and plays a pivotal role in determining the photovoltaic performance of DSCs. It is therefore interesting to synthesize complex nanostructures made of rhombus-shaped nanorods and the other nanostructures. Recently, there are some reports on the synthesis and application of Zn(OH)F nanostructures or ZnO nanostructures transformed from Zn(OH)F [19–32]. However, to best of our knowledge, the synthesis of nanostructures composed by Zn(OH)F nanorods and nanoplates has never been reported. The synthesized Zn(OH)F nanostructures can be transformed into porous ZnO nanostructures by heat treatment. The obtained ZnO nanostructures should have improved performance when used in DSCs due to the porosity of the yielded nanostructures.

3.2. Morphology and structure of the Zn(OH)F nanoplates decorated Zn(OH)F nanorod nanostructures

Fig. 2(a) and (b) shows the FESEM images of the products grown for 5 h on the FTO substrate. It clearly shows that except for some plate-like nanostructures grown on the surfaces of the nanorods, the morphology of Zn(OH)F nanorods does not change too much. This may be due the lack of Zn^{2+} ions in the solution. It is reported that the synthesis of Zn(OH)F nanorods can be finished within 1 h in a mixed solution consisting of 0.05 M $Zn(NO_3)_2$ and 0.2 M NH_4F [22]. In our experiment, a lower concentration of Zn $(NO_3)_2$ and a higher concentration of NH_4F was used (the detailed growth condition was described in the film no. 2 in Table 1). During the nanorod growth process, the concentration of the Zn^{2+} ions will decrease rapidly due to the low concentration of Zn $(NO_3)_2$ in the solution (Eqs. (1) and (2)). The lower concentration of Zn^{2+} ions in the solution can not provide enough Zn^{2+} ions for Zn(OH)F nanorod growth. As a result, the synthesis of Zn(OH)F nanoplate on the surfaces of the nanorods was realized, as represented in Fig. 2(a) and (b).

As the reaction time goes on (8 h as shown in the film no. 3 in Table 1), more and more nanoplates will grow on the surfaces of the nanorods, as shown in Fig. 3(a) and (b). Interestingly, the nanoplates are interconnected with each other to form a macroporous network. Benefiting from the favorable porous structure as well as the large surface area of the synthesized nanostructures,

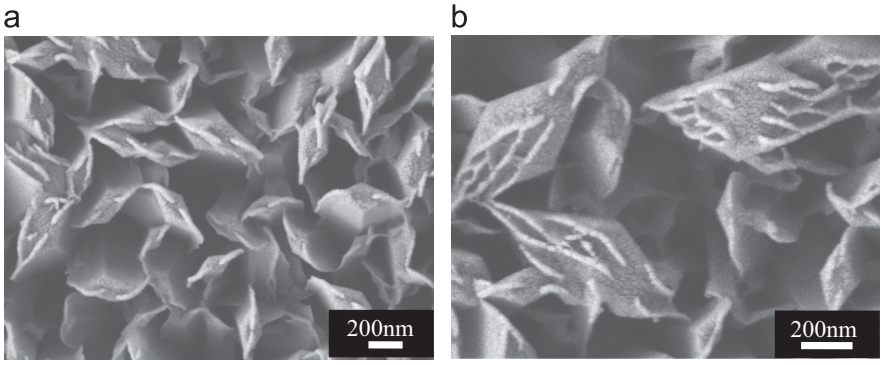

Fig. 2. (a) Low- and (b) high-magnification SEM images of the obtained rhombus-shaped Zn(OH)F nanorods with nanoplates grown on their surfaces. This sample is corresponding to the film no. 2 described in Table 1.

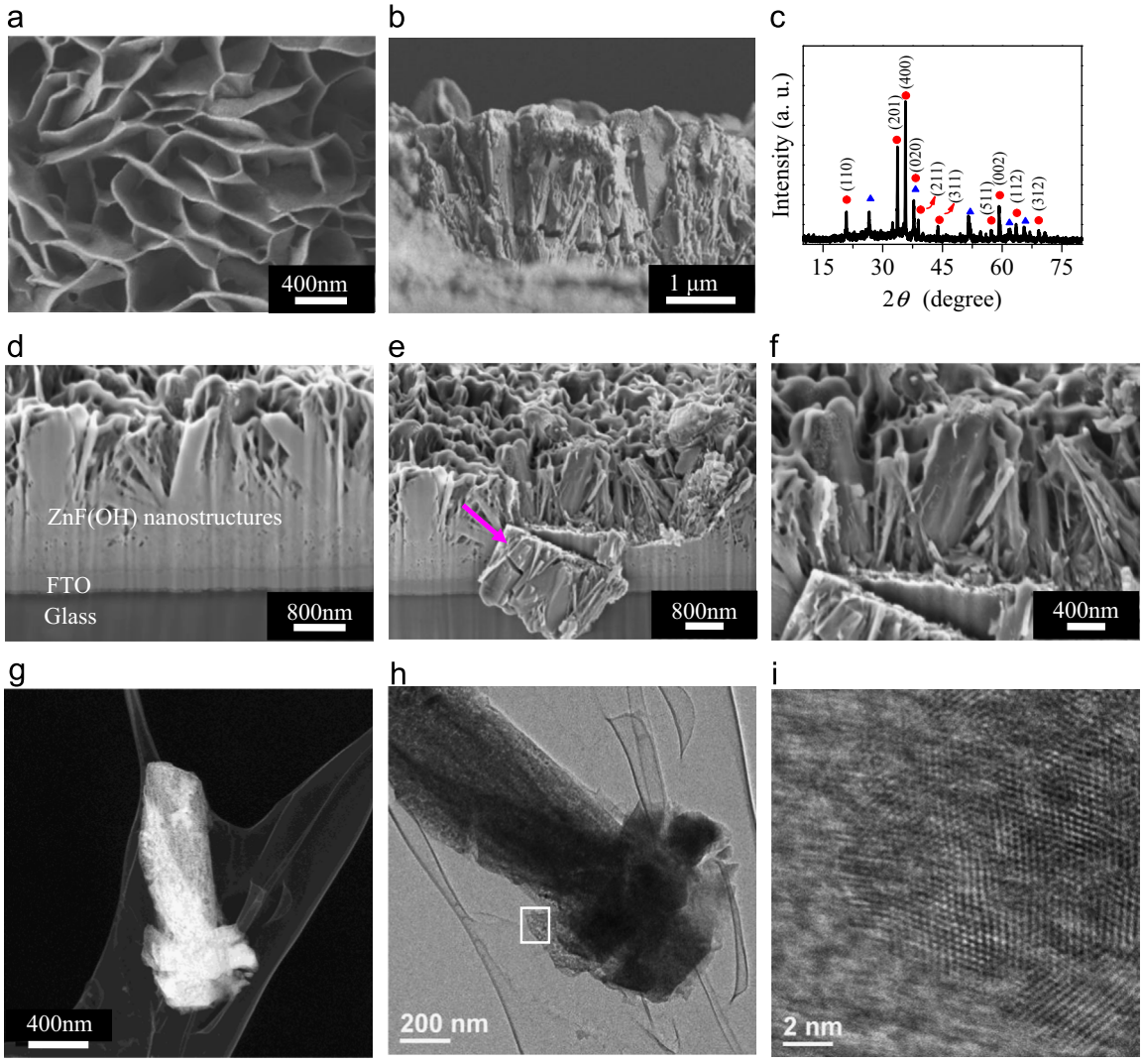

Fig. 3. (a) Top-view, (b) cross-section SEM images and (c) XRD pattern of Zn(OH)F nanoplates decorated rhombus-shaped Zn(OH)F nanorods which are corresponding to the film no. 3 described in Table 1. (d)–(f) Cross-section SEM images of the FIB-prepared sample. (g) STEM image, (h) TEM image and (i) HRTEM image of the nanoplates decorated nanorods.

the obtained nanostructures may have potential applications in DSCs, gas sensors, and photocatalysis. The XRD pattern of the novel nanostructure is shown in Fig. 3(c), which is very similar to that demonstrated in Fig. 1(a), indicating the synthesized novel nanostructures are pure Zn(OH)F.

In order to further investigate the microstructures of the hierarchical nanostructures, the FIB technique was used for cross-sectional sample preparation. As we all know, FIB sample preparation can provide a smooth cross-sectional surface particularly at the interface of different materials. The SEM image of

the cross-sectional surface is shown in Fig. 3(d). The results clearly demonstrate three discrete regions: glass, FTO layer, and the Zn(OH)F nanostructure layer. From the Zn(OH)F nanostructure layer, one can see that Zn(OH)F nanoplates were grown in the interstices among the nanorods forming a porous nanostructure. In order to reveal the morphologies of nanorods and nanoplates clearly, a probe was used to destroy the smooth cross-sectional surface. The broken area is indicated by an arrow shown in Fig. 3(e). From the high-magnification SEM image of the area represented in Fig. 3(f), one can clearly see that the complex nanostructure layer is composed of nanorods and nanoplates. Compared with the nanostructure shown in Fig. 1(d), the surface area of the complex nanostructure demonstrated in Fig. 3(f) should be increased due to the growth of nanoplate on the surface of the nanorod.

In order to investigate the microstructures of obtained products, TEM analysis was carried out. Fig. 3(g) and (h) shows the STEM and TEM image of a Zn(OH)F nanorod with the nanoplate grown on its surface, respectively. From these figures, one can clearly see that nanoplates grow on the surface of the nanorod. Fig. 3(i) shows the high-resolution TEM (HRTEM) image of the nanoplate indicated by the rectangle in Fig. 3(h). From this figure, it clearly exhibits that the nanoplate is composed of nanocrystalline grains with different orientations, indicating the polycrystalline nature of the nanoplate.

3.3. Morphology and structure of the calcinated products

The main attempt in the present work is to synthesize ZnO complex nanostructures with a large surface area for solar cell application. By calcining the obtained Zn(OH)F nanostructure precursor, ZnO nanoplates decorated rhombus-shaped ZnO nanorods can be obtained. The XRD pattern of the calcined film was shown in Fig. 4(a). It can be seen that all the diffraction peaks can be assigned to the hexagonal wurtzite structure of ZnO [JCPDS no. 36-1451]. This indicates that the as-grown Zn(OH)F nanorods and nanoplates can be transformed into a pure ZnO phase by subsequent calcining. The following chemical reaction takes place during this process:

$$Zn(OH)F \rightarrow ZnO + HF \quad (3)$$

Fig. 4(b) and (c) represents the FESEM images of the calcined products with different magnification. From the low magnification image of Fig. 4(b), it can be seen that the film has a similar thickness compared with that shown in Fig. 3(b). From the high magnification image of Fig. 4(c) and the top view SEM image shown in the inset of Fig. 4(b), one can see that no significant morphology changes can be observed after calcination.

Further structural information of the calcinated products is given by TEM analyses. The TEM images under different magnifications are shown in Fig. 4(d)–(f). The HRTEM image in Fig. 4(f) and its corresponding fast Fourier transform (FFT) pattern shown in the inset confirm there are some misorientations and defects in the porous nanostructure. From the high magnification TEM images of Fig. 4(e) and (f), one can see that some pores are embedded in the calcinated nanostructures, as indicated by the arrows shown in the two images. The porous morphology of the obtained products should originate from the release of HF during the decomposition of ZnF(OH), as expressed in Eq. (3). This interesting morphology is favorable for DSC applications. The obtained novel structure may also find potential applications in photocatalysis and gas sensors due to the fact that the existence of a porous surface enhances the photocatalytic activity and sensitivity of gas sensor [23].

3.4. Solar cell applications of the obtained ZnO nanostructures

The ZnO nanoplate decorated rhombus-shaped ZnO nanorod nanostructures (Fig. 4(b)) was introduced to DSC application and its performance was compared with that of the rhombus-shaped ZnO nanorod (calcining the products shown in Fig. 1(b)) based

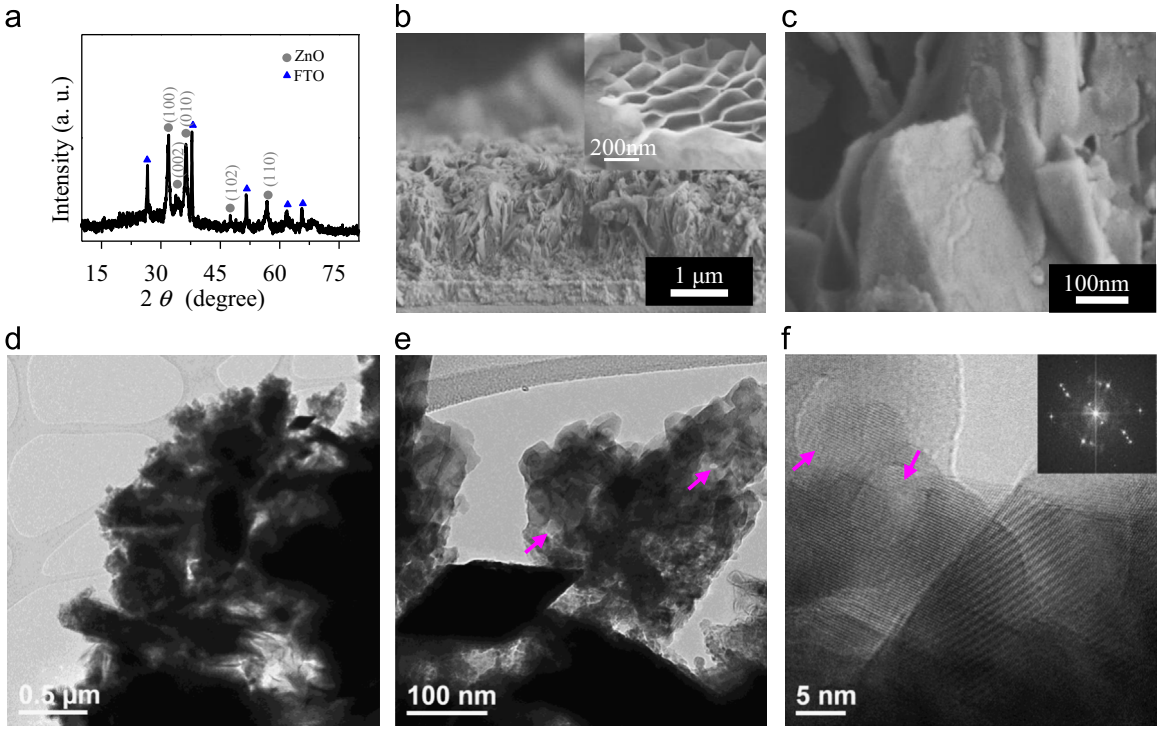

Fig. 4. (a) XRD pattern, (b) Low- and (c) high-magnification cross-section SEM image of the calcined products. The inset in Fig. (b) shows the top view SEM image of the calcined sample. (d) Low- and (e) high-magnification TEM images of the calcined sample. (f) HRTEM image of the calcined sample with the FFT pattern shown in the inset.

DSC. Fig. 5 shows the photocurrent density (J)-voltage (V) characteristics of the DSCs. The corresponding physical values including short circuit current (J_{SC}), open circuit voltage (V_{OC}), fill factor (FF) and light to electricity conversion efficiency (η), are summarized in Table 2. From Fig. 5 and Table 2, it is obvious that the solar cell constructed with the photoelectrode of ZnO nanoplate decorated rhombus-shaped ZnO nanorod exhibited a conversion efficiency of 0.85%, which is 77% higher than that of the nanorod-based DSC (0.48%). Comparing the parameters shown in Table 2 carefully, one can easily realize that the value of J_{SC} has an obvious increase, while V_{OC} and FF show little change. The increase in the short-circuit current density (from 2.16 to 3.83 mA cm^{-2}) is mainly due to the increase in the surface area of the photoelectrode by depositing nanoplates in the interstices between the nanorods and on the top of the nanorods (Fig. 3(a) and (f)).

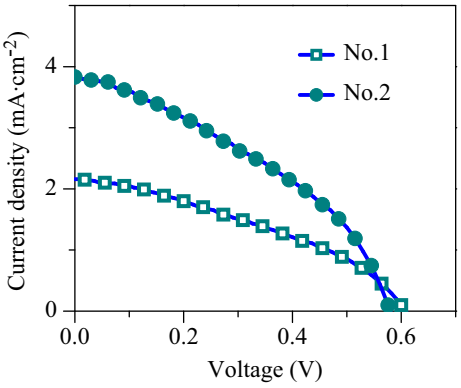

Fig. 5. Photocurrent–photovoltage characteristics of DSCs based on rhombus-shaped ZnO nanorod arrays (Photoelectrode no. 1) and ZnO nanoplates decorated rhombus-shaped ZnO nanorods (Photoelectrode no. 2).

Table 2
Photovoltaic parameters of the DSCs using rhombus-shaped ZnO nanorod arrays (photoelectrode no.1), ZnO nanoplates decorated rhombus-shaped ZnO nanorods with a film thickness of 2 μm (photoelectrode no.2) and 4.2 μm (photoelectrode no.3).

Photoelectrodes	Calcining the film shown in Table 1	J_{SC} (mA cm^{-2})	V_{OC} (mV)	Fill factor	η (%)
No. 1	Film No. 1	2.16	0.60	0.37	0.48
No. 2	Film No. 3	3.83	0.58	0.38	0.85
No. 3	Film No. 4	5.43	0.60	0.42	1.36

It is noteworthy that the film thickness of the photoelectrode used here is only 2 μm. It is reported that the efficiency of the DSC composed of hexagonal-shaped ZnO nanowire arrays increases with increasing the length of nanowires [10,11]. Qiu et al. reported that an overall efficiency as high as 1.3% was achieved with a nanowire array length of 40 μm [11]. In order to increase the length of the nanostructures on FTO substrates, a two-step growth process was adopted in our experimental process. The detailed growth condition of the step-one prepared sample has been listed in Table 1. In this step, the synthesis of highly ordered Zn(OH)F nanowire arrays on FTO substrate can be realized, as demonstrated in Fig. 1(c) and (d). In the second step, the step-one prepared sample was immersed in a fresh solution containing 0.03 M Zn $(NO_3)_2 \cdot 6H_2O$ and 0.3 M NH_4F, which was sealed in a Teflon-lined stainless steel autoclave and maintained at 120 °C for 14 h. During this process, the synthesis of nanoplate decorated nanorod nanostructures with increased thickness can be obtained.

Fig. 6(a)–(c) shows the SEM images of the obtained nanostructures. From the cross-sectional SEM image demonstrated in Fig. 6(a), one can see that nanorods are decorated by nanoplates and the thickness of the nanostructures on FTO is about 4.2 μm. Fig. 6(b) and (c) shows the top-view SEM images of the obtained nanostructures. It is obvious that large-area and high density of nanoplates have been

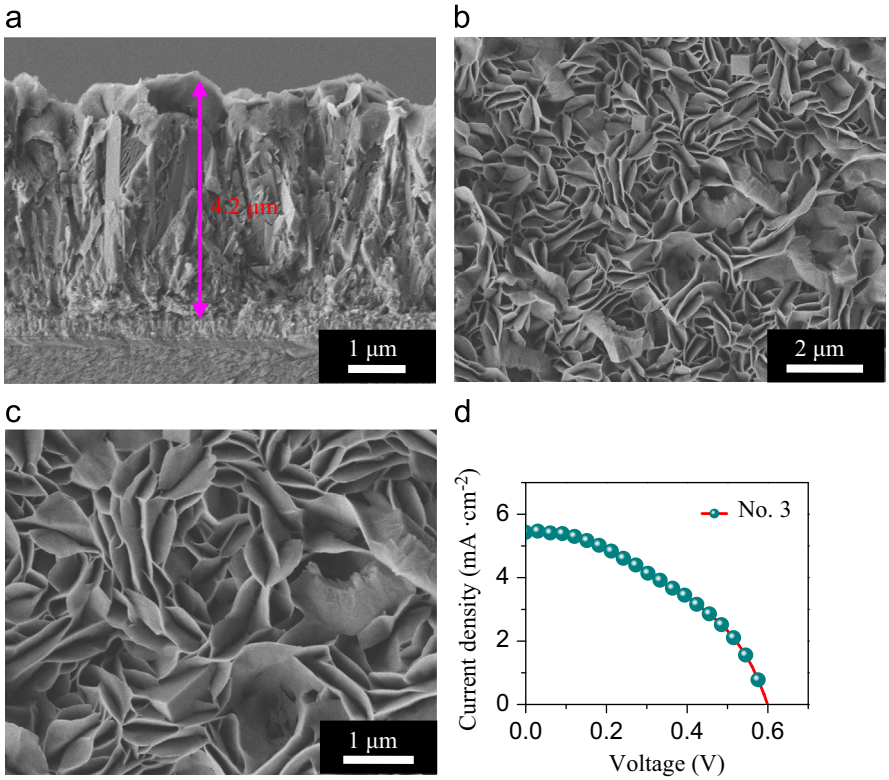

Fig. 6. (a) Cross-section SEM image, (b) low- and (c) high-magnification top-view SEM images of Zn(OH)F nanoplates decorated rhombus-shaped Zn(OH)F nanorods. This sample is corresponding to the film no. 4 described in Table 1. (d) Photocurrent-photovoltage characteristics of DSCs based on ZnO nanoplates decorated rhombus-shaped ZnO nanorods with a film thickness of 4.2 μm.

grown on the top of the nanorods. According to the above discussion, ZnO nanoplate decorated nanorods can be obtained by calcinations. After calcining, the yielded nanostructures were also used in solar cells. The resulting *J–V* curve is provided in Fig. 6(d). In order to facilitate the comparison and analysis, the corresponding physical values, such as J_{SC}, V_{OC}, FF and η have also been summarized in Table 2. From Table 2, one can see that increasing the thickness of the nanostructures on FTO leads to a significant increase in J_{SC} compared with photoelectrode no. 2. When the thickness of the nanostructure increases from 2 to 4.2 μm, J_{SC} increases from 3.83 to 5.43 mA cm^{-2}. The increase in the J_{SC} comes from the enlarged surface area in the thickened nanostructures on FTO. The increased surface area of the photoelectrode would result in enhanced dye loading. As a result, the light harvesting in the thickened nanostructure would increase, so would, the short-circuit current density and overall efficiency of the solar cell.

4. Conclusions

In conclusion, rhombus-shaped ZnO nanorod arrays and a novel porous structure of ZnO nanoplates decorated rhombus-shaped ZnO nanorods have been synthesized by a facile hydrothermal method combined with subsequent calcinations. The growth of nanoplates in the interstices between the nanorods and on the top of nanorods is considered for surface area enhancement. A preliminarily conversion efficiency of 1.36% is achieved with a 4.2 μm thick photoelectrode of ZnO nanoplate decorated rhombus-shaped ZnO nanorod array, which is comparable to those based on 40 μm vertically aligned hexagonal-shaped ZnO nanowire array counterpart, indicating the synthesized nanostructures are more suitable for application as photoelectrode in DSCs. By optimizing the thickness and architecture of nanostructures, higher conversion efficiency could be expected in the future. More importantly, the synthesized nanostructures are also expected to be used in gas sensors and photocatalysis for improved performance where a large surface area is required.

Acknowledgments

This work was supported by the National Natural Science Foundation of China (51202081), the National Major Basic Research Project (2012CB934302), the Natural Science Foundation of Jiangsu Province (BK2012244) and the College Natural Science Foundation of Jiangsu Province (12KJB430003).

References

[1] M. Thambidurai, N. Muthukumarasamy, D. Velauthapillai, C. Lee, Mater. Lett. 92 (2013) 104.
[2] L.L. Yang, Z.Q. Zhang, J.H. Yang, Y.S. Yan, Y.F. Sun, J. Cao, M. Gao, M.B. Wei, J.H. Lang, F.Z. Liu, Z. Wang, J. Alloys Compd. 543 (2012) 58.
[3] Q. Hou, L.Q. Zhu, H.N. Chen, H.C. Liu, W.P. Li, Electrochim. Acta 94 (2013) 72.
[4] M. Thambidurai, N. Muthukumarasamy, D. Velauthapillai, C. Lee, J.Y. Kim, J. Sol–Gel Sci. Technol. 64 (2012) 750.
[5] S. Jain, S.N. Sharma, M. Kumar, Physica E 44 (2011) 555.
[6] C. Dunkel, M. Wark, T. Oekermanna, R. Ostermann, B.M. Smarsly, Electrochim. Acta 90 (2013) 375.
[7] S.S. Kanmani, K. Ramachandran, J. Mater. Sci. 48 (2013) 2076.
[8] P. Uthirakumar, J.H. Kang, S. Senthilarasu, C.H. Hong, Physica E 43 (2011) 1746.
[9] M. Law, L.E. Greene, J.C. Johnson, R. Saykally, P. Yang, Nat. Mater. 4 (2005) 455.
[10] C.K. Xu, P. Shin, L.L. Cao, D. Gao, J. Phys. Chem. C 114 (2010) 125.
[11] J.J. Qiu, X.M. Li, F.W. Zhuge, X.Y. Gan, X.D. Gao, W.Z. He, S.J. Park, H.K. Kim, Y. H. Hwang, Nanotechnology 21 (2010) 195602.
[12] V.M. Guérin, J. Elias, T.T. Nguyen, L. Philipp, T. Pauporté, Phys. Chem. Chem. Phys. 14 (2012) 12948.
[13] S.B. Zhu, X.N. Chen, F.B. Zuo, M. Jiang, Z.W. Zhou, D. Hui, J. Solid State Chem. 197 (2013) 69.
[14] Y.M. Meng, Y. Lin, J.Y. Yang, Appl. Surf. Sci. 268 (2013) 561.
[15] A.B.F. Martinson, J.W. Elam, J.T. Hupp, M.J. Pellin, Nano Lett. 7 (2007) 2183.
[16] J.H. Qiu, M. Guo, X.D. Wang, ACS Appl. Mater. Interfaces 3 (2011) 2358.
[17] C.Y. Jiang, X.W. Sun, G.Q. Lo, D.L. Kwong, J.X. Wang, Appl. Phys. Lett. 90 (2007) 263501.
[18] W. Chen, H.F. Zhang, I.M. Hsing, S.H. Yang, Electrochem. Commun. 11 (2009) 1057.
[19] M. Dai, F. Xu, Y.N. Lu, Y.F. Liu, Y. Xie, Appl. Surf. Sci. 257 (2011) 3586.
[20] F. Xu, Y.N. Lu, L.T. Sun, L.J. Zhi, Chem. Commun. 46 (2010) 3191.
[21] F. Xu, L.T. Sun, M. Dai, Y.N. Lu, J. Phys. Chem. C 114 (2010) 15377.
[22] L.J. Luo, W. Tao, X.Y. Hu, T. Xiao, B.J. Heng, W. Huang, H. Wang, H.W. Han, Q.K. Jiang, J.B. Wang, Y.W. Tan, J. Power Sources 196 (2011) 10518.
[23] L.J. Zhu, Y.T. Zheng, T.Y. Hao, X.X. Shi, Y.T. Chen, J.O. Yang, Mater. Lett. 63 (2009) 2405.
[24] M. Wang, X.L. Shen, G.Q. Jiang, Y.J. Shi, Mater. Lett. 87 (2012) 54.
[25] Q.L. Huang, M. Wang, H.X. Zhong, X.T. Chen, Z.L. Xue, X.Z. You, Cryst. Growth Des. 8 (2008) 1412.
[26] Y. Peng, Chin. J. Chem. 29 (2011) 191.
[27] L.Y. Wu, J.B. Lian, G.X. Sun, X.R. Kong, W.J. Zheng, Eur. J. Inorg. Chem. 2009 (2009) 2897.
[28] X.D. Gao, X.M. Li, W. Gao, J.J. Qiu, X.Y. Gan, C.L. Wang, X. Leng, CrystEngComm 13 (2011) 4741.
[29] Y. Peng, H.Y. Zhou, Z.H. Wang, CrystEngComm 14 (2012) 2812.
[30] H.N. Chen, L.Q. Zhu, Q. Hou, W.T. Liang, H.C. Liu, W.P. Li, J. Mater. Chem. 22 (2012) 23344.
[31] X.Y. Hu, B.J. Heng, X.Q. Chen, B.X. Wang, D.M. Sun, Y.M. Sun, W. Zhou, Y.W. Tang, J. Power Sources 217 (2012) 120.
[32] J.K. Song, M.B. Zheng, Z.J. Yang, H.Q. Chen, H.Y. Wang, J.S. Liu, G.B. Ji, H.Q. Zhang, J.M. Cao, Nanoscale Res. Lett. 4 (2009) 1512.